

Part I
Basic Concepts in Crystal Growth Technology

1

Thermodynamic Modeling of Crystal-Growth Processes

Eberhard Buhrig, Manfred Jurisch, Jürgen Korb, and Olf Pätzold

1.1

Introduction

Single-crystal growth from the melt is a very complex process that can be described, analyzed and controlled by various models. Relevant models [1–9] focus on:

- temperature distribution in melt, growing crystal and growth equipment, convective flow in the melt, stress/strain field in the growing crystal including the formation of defects like dislocations;
- temperature-dependent defect inventory of the crystal;
- behavior of melt/crystal interface and atomic growth mechanisms;
- thermochemical reactions in the growth chamber.

This chapter shows current possibilities and limitations of thermodynamic/thermochemical modeling in bulk single-crystal growth. In view of the highly complex subject matter the choice of the examples makes no claim to be complete, but shall consider very different modeling applications.

The fundamentals of thermodynamics/thermochemistry in crystal-growth processes have been described by Jacobs [5] in a very comprehensive way and are assumed to be known as a basis for the following.

The complex software package *ChemSage* and its successor *FactSage* [10] that are based on a minimization of the Gibbs free reaction energy are used for the thermodynamic calculations. This software offers solutions for the entire procedure from data gathering up to process simulation. To avoid confusion with other definitions and to facilitate our own activities the *ChemSage* nomenclature is used in this chapter [11].

It should, however, be mentioned that there are also available other program packages with similar capabilities, for example, Thermo-Calc [12] or HSC Chemistry [13]. As the general approach of thermodynamic modeling does not depend on the software the application of *ChemSage*/*FactSage* is not compulsory.

Thermodynamic/thermochemical models are simplified versions of the real processes, that is, they may only reproduce aspects included in the model. The resulting limitations have to be taken into consideration for any interpretation of results. In particular, it should be emphasized that thermodynamic models only describe thermodynamic equilibrium conditions and do not include reaction kinetics.

1.2 General Approach of Thermodynamic Modeling

1.2.1 Basics

Thermodynamic modeling is a highly efficient tool that may be used to describe, develop, optimize and control crystal-growth technologies. It has, however, also the following shortcomings and limitations:

- only equilibrium conditions can be described that very seldom occur under conditions of practical relevance;
- a complete data set of all relevant species is necessary for a comprehensive description of the respective thermodynamic system;
- a highly efficient software is required for calculations.

Therefore, thermodynamic modeling is mainly applied to make statements of trend.

1.2.1.1 State Variables for the Description of Equilibrium Conditions

Thermochemical and *thermodynamic* modeling are regarded as synonyms with *thermodynamic* modeling being the preferred term in this chapter.

Thermodynamics defines thermodynamic state variables that are both independent influencing parameters and measures at the same time. The most important state variables are given in Table 1.1.

Table 1.1 State variables.

Temperature	T	In K or °C
Volume	V	In m^3 , l, dm^3
Amount	n	In mole
Concentration	c, x	Mole fraction
Pressure	P	In bar
Partial pressure	p	For ideal systems
Fugacity	f	For real systems
Surface	O	In m^2 /mole, relevant for very small particles
Energy	E	In J (magnetic, mechanical, electromagnetic, etc.)

Reactions between the components of a thermodynamic system can be characterized by thermodynamic state functions (thermodynamic potentials) depending on state variables. The most important state function in thermodynamic modeling is the Gibbs free energy (G) that defines

- the equilibrium state of a system;
- the capacity for doing chemical work;
- the chemical potential of substances;
- the direction of chemical reactions;
- the magnitude of the driving force for chemical reactions.

The Gibbs free energy is given by

$$G = H - T \cdot S \quad (1.1)$$

with H , enthalpy, T , temperature and S , entropy.

It can be split into several terms:

$$G = G^{\text{ref}} + G^{\text{id}} + G^{\text{ex}} \quad (1.2)$$

with the following meanings:

- G^{ref} , reference values of pure substances at $T = 298.5 \text{ K}$ and $P = 1 \text{ bar}$ taken from databases;
- G^{id} , Gibbs free energy of an ideal system in dependence on state variables;
- G^{ex} , deviation from ideal behavior in a mixed system.

For the excess Gibbs free energy G^{ex} the model of a sub-regular solution according to Redlich–Kister–Muggianu [14] is used in this chapter. It is valid for binary i - j interactions in multi-component systems.

$$G_{ij}^{\text{ex}} = x_i x_j \sum_v L_{ij}^{(v)} (x_i - x_j)^{(v)} \quad (1.3)$$

$L^{(v)}$, interaction parameter

x , concentration

If necessary, a fourth member, the so-called *constrained power operator*, can be added to Equation 1.2 by which additional influencing parameters like magnetic or electric fields, electrolytic potentials as well as time-dependent aspects of single reactions may be integrated into the model [15].

1.2.1.2 The ChemSage Software Package

The commercial *ChemSage* software package has been developed by Gesellschaft für Technische Thermodynamik und -physik GmbH [16]. This package allows for the complete thermodynamic modeling of complex crystal-growth processes. A schematic overview of the ChemSage family is given in Figure 1.1.

The actual thermodynamic calculations for all program members take place in the central module (solver), the Gibbs free energy minimizer. This module is not accessible to users.

ChemApp [17] is a freely accessible programming platform which allows for programming of peripheral applications and online connection to external programs of global models, for example, crystal-growth processes.

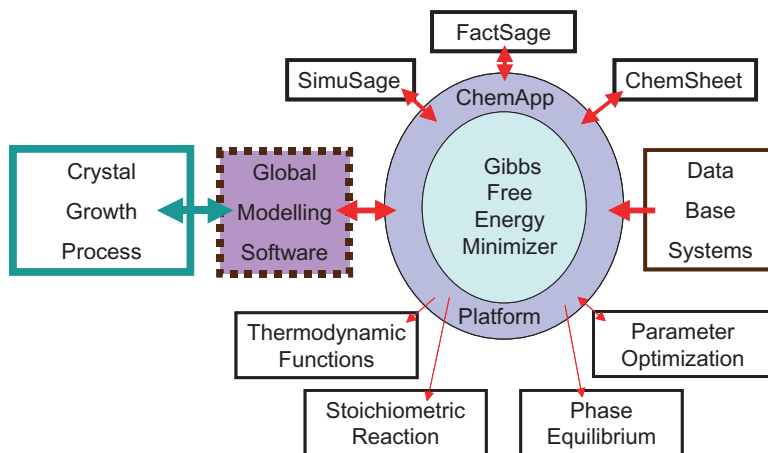


Figure 1.1 The *ChemSage* family.

In the following, the *FactSage* program is preferentially used. With this program it is possible to realize numerical calculations, graphical representations and input/output procedures, as well. *FactSage* also allows for connections with international database systems by which the standard values of the Gibbs free energy can be obtained for all relevant species of the investigated system.

In addition, the following modules belong to the *ChemSage* family:

- *SimuSage*, a software for interactive simulation of processes;
- *ChemSheet*, a software for handling input/output operations including all functions of the *Excel* software. Even externally programmed processes like diffusion or other time-dependent procedures can be integrated by *ChemSheet*.

Furthermore, the *ChemSage* family comprises an effective module for optimization of thermodynamic data by which missing initial data can be added or adjusted. Finally, a thermodynamic model of a reactor is available that allows for simulations of pseudo-3D and time-dependent processes.

In the following, there are given some examples for the calculation of realistic thermodynamic functions of single-species and stoichiometric reactions as well as calculations of many-component, many-phase equilibria.

The first example will be considered in detail in order to demonstrate the single steps of thermodynamic modeling, whereas the remaining ones are illustrated in an abbreviated form, as the general approach is always the same.

1.3

Crystal Growth in the System Si–C–O–Ar (Example 1)

The first step of modeling is the detailed formulation of the task and the selection of the components relevant for the system.

In the following, a special aspect of thermal silicon technology will be shown. The system components are Si, C, O and Ar chosen because of their practical relevance:

- metallurgical silicon can be obtained from silicon oxides and carbon containing components in an electrical arc furnace (Si–O–C);
- silicon single crystals of electronic purity are grown under vacuum or in an Ar atmosphere by the Czochralski method from fused silica crucibles supported by graphite containers;
- silicon single crystals can also be grown by the floating zone technique under vacuum or argon protective gas;
- silicon sheets are produced by the EFG (edge-defined film-fed growth) process using graphite crucibles and graphite shapers;
- ingot casting of silicon for solar cell production.

In any case, the quality of silicon is mainly determined by carbon and oxygen impurities.

1.3.1

Selection of Species

As a rule, there are different and sometimes contradictory data for a given number of components of existing species and their modifications in international databases or publications. For this reason, a constrictive selection has to be made as the next step (Table 1.2).

1.3.2

Test Calculation, Check of Consistency

The next steps are test calculations and check of data consistency. As an example, the calculated Gibbs free energies for 1 mole of the stoichiometric condensed phases of the system at 1413.85 °C and 1 bar are compiled in Table 1.3. Despite

Table 1.2 Species in the Si–C–O system under Ar as a possible protective gas.

Stoichiometric, condensed phases	C, SiO ₂ , SiC
Solid solution phase	Si(s) containing O and C
Liquid solution phase	Si(l) containing O, C
Gas phase	Containing SiO ₂ , SiC, Ar, SiO, CO, Si, Si ₂ C, Si ₂ , Si ₃ , CO ₂ , Si ₂ O ₂ , SiC ₂ , O, O ₂ , C ₂ O, C (with a cut-off pressure of 2×10^{-16} bar)

Table 1.3 Gibbs free energy of selected condensed phases (original print).

Constituent	Heat capacity	Enthalpy	Entropy	Gibbs energy
	J K ⁻¹	J	J K ⁻¹	J
1 mol of Si (l)	2.71960E + 01	8.62502E + 04	9.15688E + 01	-6.82264E + 04
1 mol of Si (s)	2.92224E + 01	3.60422E + 04	6.17975E + 01	-6.82102E + 04
1 mol of SiC (s)	5.20217E + 01	-7.50157E + 03	9.01619E + 01	-1.59605E + 05
1 mol of SiO ₂ (s)	7.36727E + 01	-8.13803E + 05	1.55336E + 02	-1.07585E + 06

Original print

T = 1413.84987051 °C, P = 1.00000E + 00 bar.

the different molecular weights the numerical values of the Gibbs free energies allow the following statements to be made:

- the Gibbs free energy of solid and liquid silicon are equal, that is, Si(l) and Si(s) are in thermodynamic equilibrium at a temperature of 1414.85 °C, defining the crystallization/melting temperature characteristic for the data set,
- the Gibbs free energies of SiO₂ and SiC are more negative than G for Si(l) and Si(s), that is, a reaction including silicon is impossible as long as free carbon or oxygen exist in the system,
- SiO₂ has a more negative Gibbs free energy compared with SiC, that is, oxygen suppresses carbon in silicon carbon compounds (at the given temperature).

In this way, the existence of all species of the model system can be roughly assessed as a function of temperature and pressure. The actual stability of species can, however, only be defined by a thermodynamic equilibrium calculation of the complete system or of single chemical reactions (see next item).

1.3.3

Calculation of Gibbs Free Energy for Selected Reactions

At high temperatures, permanent reactions take place between the individual species and phases of the model system. Therefore, dynamic equilibria will be calculated the status of which depends on temperature and concentration of species/components. As an example, the adjustment of the dynamic equilibrium for the single reaction of oxygen containing liquid silicon and gaseous SiO will be considered. The reaction scheme is displayed in Figure 1.2.

The temperature of 1414 °C just above the melting point of silicon (see Table 1.3) has been chosen. Using *FactSage* a negative Gibbs free energy of the reaction dG is obtained, that is, gaseous SiO is spontaneously formed. From the equilibrium constant describing the ratio of the oxygen activity in liquid silicon to the

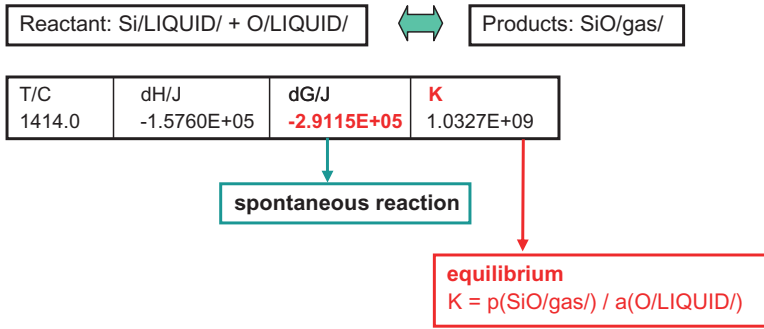


Figure 1.2 Reaction of liquid silicon with SiO.

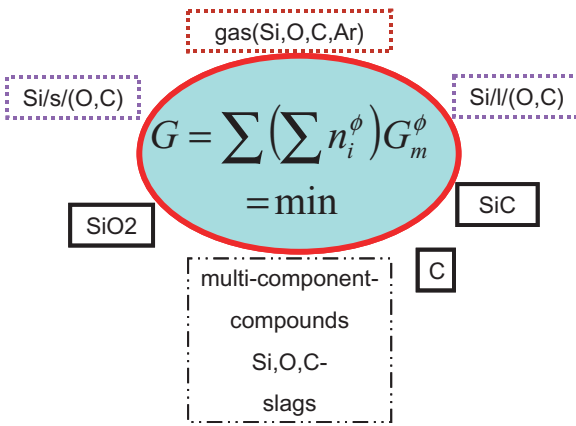


Figure 1.3 Principles of G minimization in the model system Si-C-O-Ar, G_m^ϕ , molar integral Gibbs free energy of phase ϕ , n_i^ϕ , mole number of the constituents i of phase ϕ .

activity of SiO in the gas phase it follows that there always exists a SiO partial pressure over oxygen-containing silicon.

1.3.4 Minimization of Gibbs Free Energy of Complex Systems

The calculation of Gibbs free energies of single components as well as the calculation of dG values for single reactions in a complex system is incomplete in the sense that in a multi-component system all species react with each other and an equilibrium state will occur. For the calculation of such a complex equilibrium a minimization of the Gibbs free energies of the entire system is necessary with consideration of concentrations, activities and partial pressures of all species in all phases. This procedure is schematically depicted for the model system Si-C-O-Ar in Figure 1.3. Slugs have not been considered in these calculations.

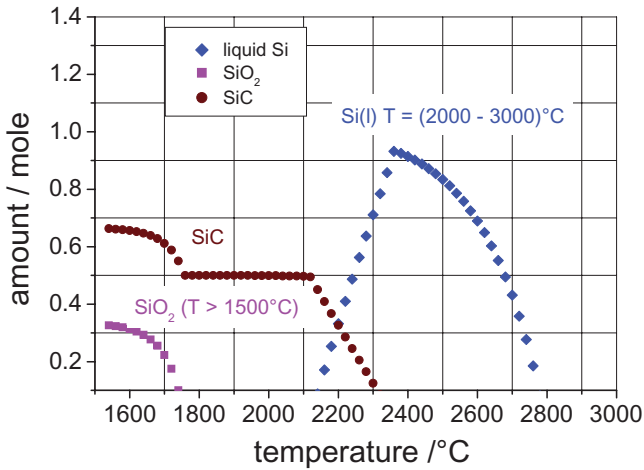


Figure 1.4 Condensed phases in the high-temperature reactor.

The question to be answered next is: What are the conditions for the production of elementary silicon in a high-temperature reactor? The high-temperature reactor for the production of metallurgical silicon could be an electrical arc furnace. One of the reactions that take place is:



The results of the calculations are graphically represented in Figure 1.4. The temperature-dependent coexistence of the condensed phases are given. Elemental silicon does not exist below 2100°C, instead there are SiO₂, SiC or C. At temperatures above 2100°C elemental liquid silicon is formed. The amount of silicon increases up to a maximum at a certain temperature. The following decrease of the amount of liquid silicon is caused by the increasing evaporation of silicon, that is, the transition into the gas phase. This is evident from Figure 1.5 representing the partial pressures of different species in the gas phase.

These calculations provide a first approximation of the conditions for the carbo-chemical production of silicon. A refined and more realistic thermodynamic description of the process requires the application of the above-mentioned reactor model. This has been demonstrated by Hack in [11].

1.3.5

The Thermodynamic-Technological Model of the Edge-Defined Film-Fed Growth of Silicon

In the above-discussed example the reactor is regarded as a black box without geometrical constraints. As an example of a geometrically structured thermodynamic-technological model the production of thin silicon ribbons by edge-defined

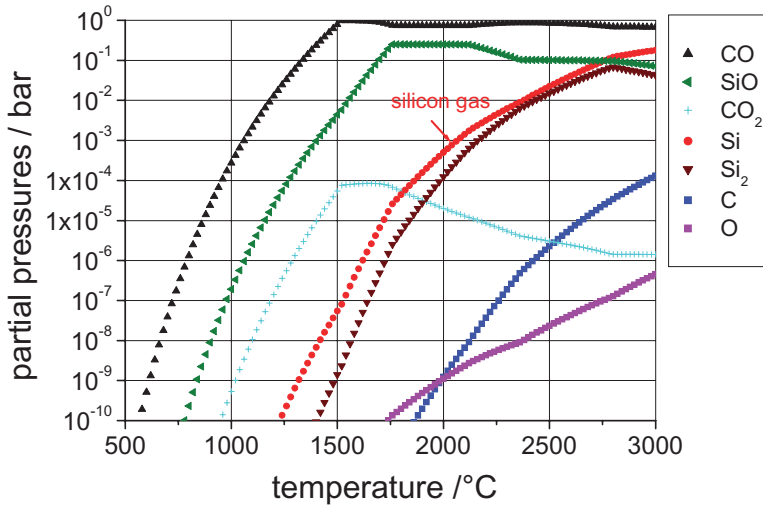


Figure 1.5 Partial pressures of species.

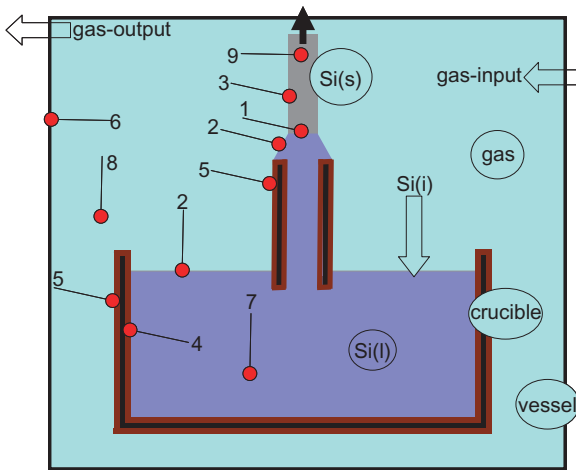


Figure 1.6 Technological model of Si-EFG.

film-fed growth (EFG) [18] is considered. A schematic cross-section of a EFG reactor is shown in Figure 1.6. It is not the real reactor, but provides the basis for a description of possible chemical reactions.

The process is performed in a closed reactor filled by an argon protective gas of about 1 bar. The crucible consists of graphite and is continuously charged with granulated silicon. The silicon ribbon is formed by a graphite shaper and is continuously drawn upwards at a certain rate. As the silicon granules are covered by SiO_2 , oxygen is incorporated in the charge as an impurity. A second source of

oxygen impurity is the flushing with argon protective gas. Therefore, an accumulation of oxygen impurities will take place in the course of the process.

- Again, Si–C–O–Ar are the components of the systems. The species and phases are the same as given in Table 1.2. Inside the melt there are different temperatures: the highest at the graphite crucible (4), the lowest at the phase boundary between liquid and solid silicon (1). Without going into detail the thermodynamic calculations show the following:
- at position (1) in Figure 1.6 crystallization takes place characterized by the corresponding distribution coefficients of oxygen, carbon and other impurities:

$$k = \frac{\text{Si(s)}(\text{O}, \text{C})}{\text{Si(l)}(\text{O}, \text{C})}; \quad (1.5)$$

- at position (2) reactions between oxygen and carbon with the liquid silicon occur and the vessel is filled by reaction products;
- reactions between the gas atmosphere and solid silicon take place at positions (3), where either SiO₂ or SiC are formed depending on the chemical condition in the gas phase;
- at position (4) a reaction between the graphite crucible and liquid silicon is indicated, leading to a more or less closed SiC layer and an incorporation of carbon into liquid silicon;
- the outer surface of the graphite crucible (5) is likewise covered by SiO₂ or SiC due to O- and C-containing species in the gas atmosphere;
- condensation of SiO₂ and SiC, but also of Si (6) take place at the cold container wall;
- position (7) indicates a possible homogeneous precipitation in liquid silicon caused by a temperature and/or concentration supersaturation;
- the possible formation of solid or liquid particles in the gas phase is marked at (8);
- the possible precipitation in solid silicon during cooling down of the ribbon is indicated at (9).

At all positions mentioned above it is possible to optimize the process or to analyze negative effects.

In the following some results of the calculations are described.

As a first example, the evaporation of Si species from a Si melt at a temperature of 1414°C in a reactor filled with argon at 1 bar is considered (Figure 1.7). The model describes the start of the process after melting of solid silicon. The calculation has been performed in such a way that an increasing amount of silicon was injected in a given volume. Three Si containing species are formed: Si, Si₂ and Si₃. The dominating species is Si, the amounts of Si₂ and Si₃ are lower by two orders of magnitude. By varying the Si amount (*x*-axis) equilibrium pressures between

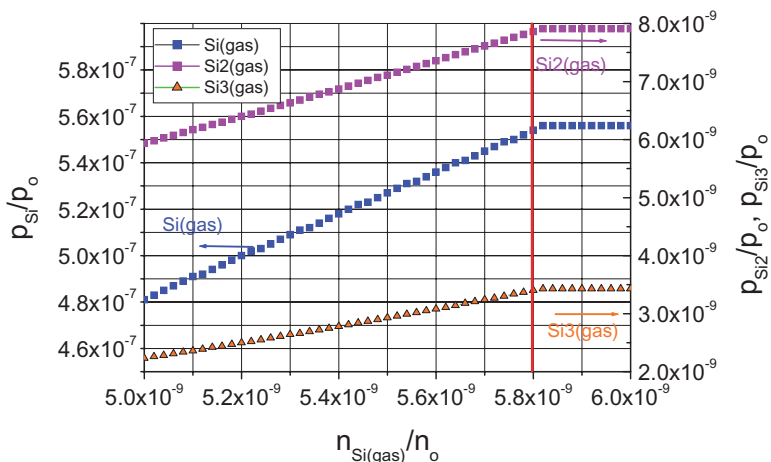


Figure 1.7 Evaporation of Si species into an Ar-filled reactor (p_o , reference pressure, n_o , reference amount).

Si, Si₂ and Si₃ species and the melt are reached at a value of 5.8 E–09 (vertical line in Figure 1.7). At this point, the gas phase is saturated by all of the Si containing species. A further increase of the total amount of silicon in the gas phase, for example, by an input of gaseous Si would result in a condensation of species and in an increase of the amount of liquid silicon.

The rate of equilibrium establishment is determined by the kinetics of evaporation/condensation as well as diffusion and convection in the system.

The next calculation deals with the influence of carbon in the crystallizer. The initial state of the system (1414 °C, 1 bar) is characterized by liquid and solid silicon in mixed phases and the Ar gas phase containing Si, Si₂, Si₃, C, C₂, C₃, SiC and SiC₂ as dominant species in the gas phase. The liquid and solid silicon contain carbon as the main constituent.

The addition of carbon can be realized in the *ChemSage* program by injecting carbon into the gas phase, by feeding of C-containing silicon or by dissolution of a carbon source (e.g., graphite from the internals). As can be seen from Figure 1.8, the C content of liquid and solid silicon increases with increasing C injection, at first without generation of a new phase. At the same time the carbon content of the mixed gas phase, that is, is the partial pressures of corresponding species increase (not displayed in Figure 1.8 for the sake of clarity). Each carbon content in liquid silicon corresponds to an equilibrium C content in solid silicon as well as in the gas phase.

At a critical amount of carbon (1.1×10^{-8} mole in the model) solid carbon carbide, SiC, is formed as a new phase. A further increase of the amount of carbon does not change the carbon content in the liquid and solid silicon as well as in the gas phase, but the amount of SiC will increase. The SiC forms a layer on the surface of liquid or solid silicon or precipitates in the volume of the phases.

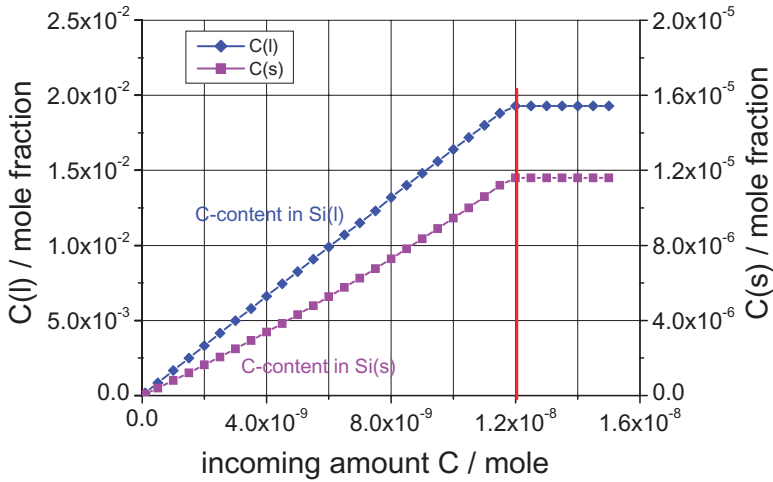


Figure 1.8 C injection in the system.

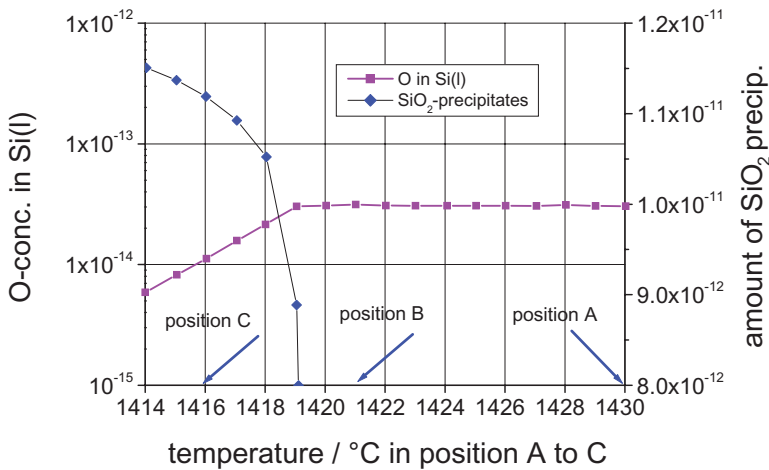


Figure 1.9 Oxygen content of liquid silicon in dependence of temperature. The data applied for the calculations were taken from SGTE pure substances database, version 2007.

In the next example the homogeneous reaction between oxygen and liquid silicon is considered as a function of temperature (Figure 1.9).

A confined region of the thermodynamic system (e.g., a chemically insulated region without phase boundaries) shall be contaminated by an oxygen-containing gas phase or oxygen loaded silicon at a temperature of 1430°C (“position A” in Figure 1.9). We assume that this insulated region will be transported without material exchange with the surroundings to a region of lower temperature, for

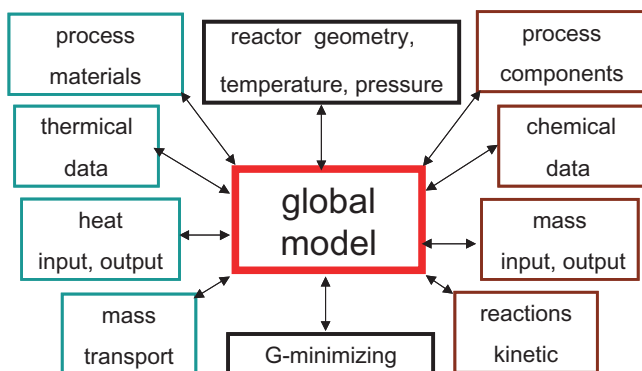


Figure 1.10 Global model of crystallization.

example, in the direction of the melting temperature of 1414°C (“position C” in Figure 1.9). At first, during the transition to lower temperature the content of oxygen in the melt does not change. At the temperature marked by B in Figure 1.9 precipitation of SiO_2 starts assuming that no supersaturation is necessary. The amount of precipitated SiO_2 increases with further decreasing temperature reaching a maximum at the crystallization temperature of silicon (“position C” in Figure 1.9). The precipitates are possibly incorporated into the growing Si crystal. They can be the reason for the formation of structural defects up to the transition to polycrystalline growth. The formation of SiO_2 precipitates can only be suppressed by a reduction of oxygen content in liquid silicon below the solubility limit. An accumulation of SiO_2 precipitates is possible especially in the capillary region of the EFG crystallizer.

The above-discussed 3 examples supply qualitative statements only. To get quantitative results precise technological parameters like amounts, concentrations, volumes, etc., have to be used.

Nevertheless, to ensure that results will be feasible and more realistic, thermodynamic equilibrium calculations have to be supplemented by a global model of the process. This global model should combine the precise process parameters with the thermodynamics and kinetics of the process as well as with the transport of heat and mass in the system. Such a global model is outlined in Figure 1.10.

Solutions for components of the model are already available. The integration of these components into a global model is, however, a task for the future.

1.4 Crystal Growth of Carbon-Doped GaAs (Example 2)

A thermodynamic-technological model of SI (semi-insulating) GaAs growth has to consider:

- a) the chemical reactions between the GaAs input, the construction elements and the auxiliary materials (boron oxide, crucible and impurities in the growth system);
- b) the inventory of defects in the GaAs crystal which depends on the “freezing process” of defects after crystallization and determines the application-oriented properties.

SI behavior of GaAs (e.g., [19]) occurs if the condition $N_{\text{EL2}} > [\text{C}] - (N_{\Sigma\text{SD}} - N_{\Sigma\text{SA}}) > 0$ is fulfilled. N_{EL2} and $[\text{C}]$ are the EL2 content and the concentration of intentionally doped carbon, respectively, and $(N_{\Sigma\text{SD}} - N_{\Sigma\text{SA}}) \approx 10^{14} \text{ cm}^{-3}$ is the concentration of impurities acting as shallow acceptors (SA) and shallow donors (SD). EL2 is an intrinsic mid-gap double donor, most probably a single arsenic antisite atom As_{Ga} [20] controlled by the composition in the homogeneity range of GaAs. If the content of residual impurities can be considered to be low, the carrier concentration, and thus the electrical resistivity of SI GaAs is determined by the carbon concentration.

As a first approach, a thermodynamic analysis of the complex reaction system has been performed to establish a control procedure for carbon during LEC (liquid encapsulated Czochralski) growth or VGF (vertical gradient freeze) growth of SI GaAs. The reaction system comprises the gas atmosphere, the boron oxide encapsulant, solid and liquid GaAs, the pBN crucible and the graphite heaters. Again, transport of reactants in the fluid and solid phases is neglected. A fast reaction kinetics at phase boundaries is assumed. The temperature of the system is held at the congruent melting point of GaAs (1509.42 K).

The technological model presumes that

- the phases in the system (GaAs, B_2O_3 , BN, gas) participate at the adjustment of the equilibrium with their entire volumes;
- the boron oxide coverage avoids a direct transition of elemental arsenic gas bubbles from the GaAs melt to the gas phase;
- the graphite heater does not influence the thermodynamics of the system;
- the pressure of the protective N_2 gas varies between 2 and 80 bar.

1.4.1

Components and Species in the System

The system contains the components Ga, As, B, C, O, H, Ar or N. The species considered in the calculations are summarized in Table 1.4.

The gas phase is considered as an ideal mixture of components and species. The liquid phases are regarded as sub-regular solutions according to the above mentioned Redlich–Kister–Muggianu model [14] with interaction coefficients between the main components and impurities and between the impurities. The interaction coefficients were deduced and/or approximated by adjusted thermodynamically relevant experimental data like phase diagrams. Details are given in [21]. An ideal behavior of dissolved impurities/dopants like C, N, B, O, etc., in solid GaAs is assumed as a first approximation (see below).

Table 1.4 Species and phases in the Ga, As, B, C, O, H, Ar or N system.

Stoichiometric phase	BN
Solid solution phase	GaAs(s) containing C, O, B, N and H
Liquid solution phase	GaAs(l) containing C, O, B, N and H as mixed phase with variable As/Ga-ratio
Liquid solution phase	B ₂ O ₃ (l) containing As ₂ O ₃ , As ₂ O ₅ , Ga ₂ O, GaO, Ga ₂ O ₃ , CO, CO ₂ , HBO ₂
Gas phase	N ₂ , H ₂ , Ga ₂ O, H ₂ O, BHO ₂ , GaOH, AsH, Ga, CO, AsN, B ₂ O ₃ und GaH (ranked according to the partial pressure with a cut-off pressure of 1×10^{-15} bar)

Graphite in the system requires separate consideration. If graphite is present the carbon activity under thermodynamic equilibrium conditions will be $a_C = 1$ because a Boudouard-type and other reactions are possible at the graphite heater. This would result in the saturation concentration of carbon in all phases of the system. However, GaAs single crystals grown in a graphite-containing system exhibit variable concentrations of carbon. Therefore, it is assumed that the local separation of the graphite heater and the GaAs melt and the low transport rate of carbon-containing species in liquid boron oxide are the reason for this discrepancy. As a consequence, graphite has to be excluded from the system in the case of thermodynamic equilibrium calculations of carbon incorporation.

1.4.2

Results

As pointed out by Oates and Wenzl [22] the results of the calculations can be best visualized as so-called *predominance area diagrams* as mainly redox equilibria are of importance. In the *predominance area diagram* the stability region of the GaAs melt is represented in the presence of the boron oxide encapsulant at the GaAs melting temperature of 1509.42 K in a plot of $\log(a_C)$ over $\log(p_{O_2})$ with a_C and p_{O_2} being the activity of carbon and the oxygen partial pressure, respectively (Figure 1.11). On the right-hand side of the diagram the scale of carbon concentration in the melt is given using the known activity coefficient of carbon in GaAs melt. The stability region of GaAs melt/liquid boron oxide that is essential for crystal growth is bounded by the dissociation of boron oxide at lower and the oxidation of Ga in the GaAs melt at higher oxygen chemical potentials. The upper boundary of the stability region is given by the solubility limit of carbon in liquid GaAs ($a_C = 1$). If the chemical potentials of the control species carbon and oxygen in this stability region are fixed, no degrees of freedom will be left in the system.

The chemical potentials of carbon and oxygen can be controlled by the partial pressures of CO and N₂. Nitrogen reacts with the boron oxide encapsulant forming solid boron nitride and oxygen [23]. Taking into account the possible N₂ pressure

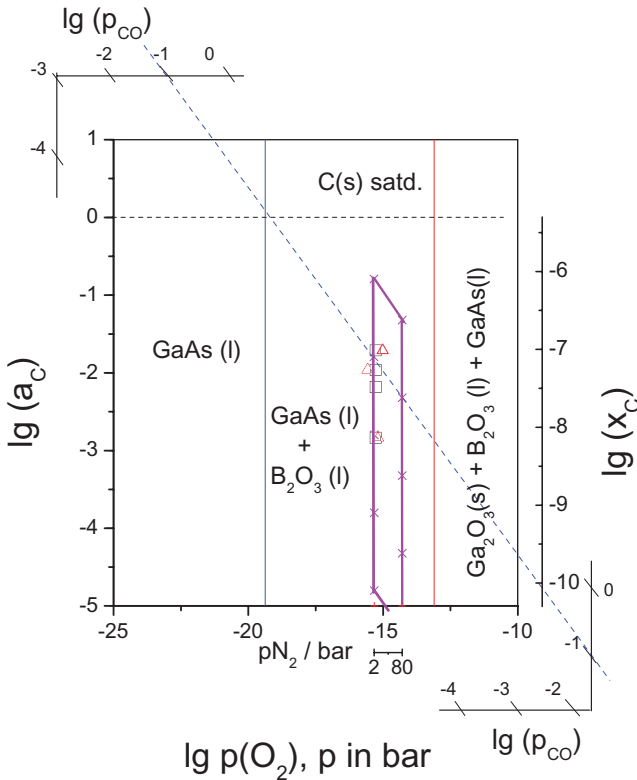


Figure 1.11 Predominance area diagram for LEC growth assuming oxygen control by nitrogen reaction with boron oxide.

in the growth equipment only a part of the stability region of GaAs(l)/B₂O₃(l) can be used for crystal growth. This working area under the assumption that the N₂ pressure varies between 2 and 80 bar is marked. The dotted line in Figure 1.11 indicates a constant CO partial pressure. It is obvious that it is not sufficient to keep the CO partial pressure constant to define the carbon content in the GaAs melt. The oxygen chemical potential must be kept constant, too. This sometimes has been ignored in the past.

A distribution coefficient $k_C = 2$ is used for the estimation of the carbon concentration in solid GaAs from the calculated C content in the melt. Likewise, the concentrations of B, O, N, H in solid GaAs are calculated by means of the corresponding distribution coefficients.

The data points in Figure 1.11 indicate experimental results observed in VGF growth at different CO partial pressures and constant oxygen potentials. They were obtained from measurements of carbon concentration in GaAs single crystals using the above distribution coefficient.

Table 1.5 Species of the SUBS model of solid GaAs.

Ga-sublattice	As-sublattice	3rd sublattice	4th sublattice
Ga_1	As_2	As_3	Va_4<0>
As_1<0>	O_2<0>	Va_3<0>	e
As_1<+>	O_2<->		h
Va_1<0>	O_2<+>		
Va_1<3->	C_2<->		
Si_1<+>			
Zn_1<->			
B_1			

Based on the results of the thermodynamic analysis a more sophisticated model has been developed by Eichler *et al.* [24] taking into account transport in the fluid phases.

1.4.3

Extended Model

For a more realistic description of solid GaAs a sublattice model (SUBS) has been developed [27] and included into ChemSage. It is based on the SCPBE model (species chemical potential–bond energy model) introduced by [25, 26] and avoids the assumption of a stoichiometric solid GaAs.

The SUBS model of crystalline GaAs consists of 4 sublattices: the Ga and As sublattice and a sublattice of interstitial atoms and one occupied by electrons and holes. In the nomenclature of ChemSage the Ga sublattice contains: Ga_1, As_1<0>, As_1<+>, Va_1<0>, Va_1<3->, Si_1<+>, Zn_1<-> and B_1, that is, arsenic antisites, Ga vacancies, Si, Zn and B atoms. They can exist in different charge states that are given in angle brackets. The constituents of the other sublattices are summarized in Table 1.5. Vacancies in the As sublattice are not considered. The interstitial sublattice contains arsenic and vacancies, only. In agreement with the crystallographic structure of GaAs, the Ga and the As sublattice have the same number of lattice sites. The defects considered in the model reflect current knowledge, but other defects can be included too, if necessary.

The positions of the localized states in the bandgap are displayed in Table 1.6 defining the midgap energy as the reference energy. E_g is the temperature-dependent energy gap. The negative U behavior of oxygen in the arsenic sublattice could not be considered in the model. Instead, it has been described by two neighboring levels resulting in the known effective level at $E_c - 0.36$ eV. A Fermi-level effect has not been considered.

The minimization of the Gibbs free energy for the calculation of the equilibrium concentrations of the species has been carried out under the conditions that the number of sublattice sites is constant and charge neutrality is fulfilled. The

Table 1.6 Localized states (relating to the middle of the bandgap E_g).

Defect	Level in the bandgap J/mol	Level in the bandgap eV
As_1<+/0>	4 000	0.041
C_2<- /0>	$-E_g / 2$	$-E_g / 2$
O_2<+/0>	34 000	0.35
O_2<0/->	35 000	0.36
Va_1<0/3->	-60 000	-0.62
Zn_1<0/->	$-E_g / 2$	$-E_g / 2$
Si_1<+/0>	$+E_g / 2$	$+E_g / 2$

chemical potentials of the sublattice species have been calculated using the SCPBE model that supplies expressions for mixing enthalpies (interaction between the defect and the Ga and As atom, respectively) and mixing entropy. Standard species chemical potentials for charged species are derived from standard species chemical potentials for neutral species and the defect levels in reference to midgap. For the threefold-occupied vacancy in the Ga sublattice it is written for example, $\mu_{\text{Va}_1<3->}^0 = \mu_{\text{Va}_1<0>}^0 + E<0/3->$ with $E<0/3->$ being the electronic transition level given in Table 1.6. The interactions between the defects in different charge states were not considered. As there shall be modeled the influence of carbon doping on resistivity of semi-insulating GaAs, the positions of the shallow defects are set to $\pm E_g/2$ without substantial error. Further details can be found in [27].

To account for the decreasing mobility of lattice species with decreasing temperature a freezing temperature is introduced. An adjustment of thermodynamic equilibrium is possible up to this freezing temperature, only. Below this temperature lattice defects are frozen, that is, the sum over the different charge states of a single defect is constant. But charge reloading is possible. The freezing temperature is dependent on the cooling conditions of solid GaAs.

This model has been used for the calculation of the homogeneity range of solid GaAs (without impurities). The result is shown in Figure 1.12. The thermodynamic data of the As antisite have been adjusted so that its concentration is roughly in agreement with the measured EL2 concentration in solid GaAs at room temperature. A constant pressure of 1 bar has been assumed.

For the native defects included in the model (Table 1.5) the calculated homogeneity range is bounded by the stoichiometric composition at lower temperatures and is extended to the arsenic-rich side. A retrograde solidus is observed. It describes the experimental result that arsenic precipitates can be formed during cooling to room temperature, depending on the starting composition of the melt and the resulting solid GaAs. The maximum solid solubility is found to be about 1180 °C, the corresponding As concentration of off-stoichiometric GaAs remains unsure because an experimental verification is not yet possible due to the insufficient accuracy of available analytical methods.

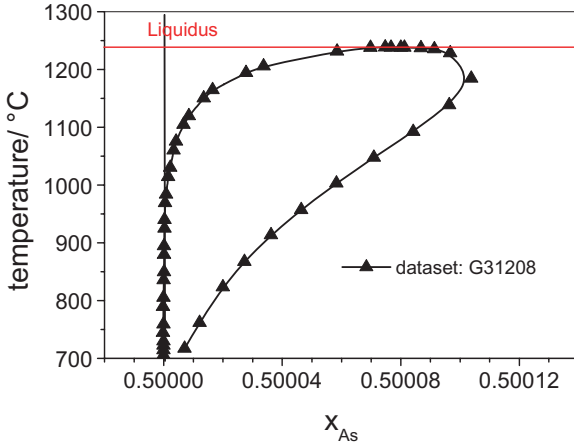


Figure 1.12 Homogeneity range of GaAs.

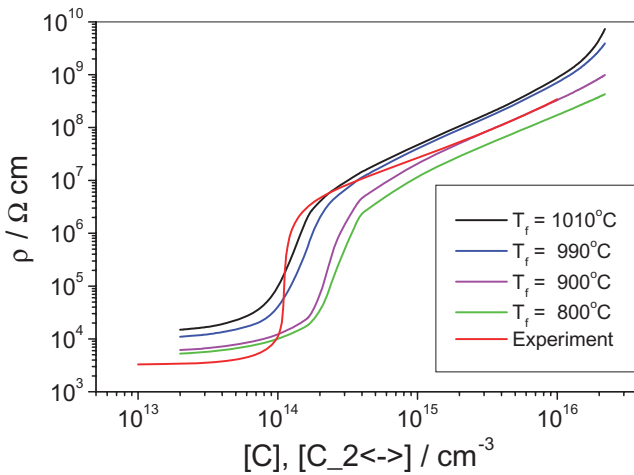


Figure 1.13 Room-temperature electrical resistivity of GaAs in dependence on C concentration for different freezing temperatures.

It should be mentioned that a slightly larger homogeneity range and a lower temperature of maximum solubility is obtained if the assumption $p = 1$ bar is replaced by the actual As pressure at the three-phase equilibrium GaAs(s)-GaAs(l)-As vapor.

In a second example of the application of the SUBS model the electrical resistivity of GaAs at room temperature is calculated in dependence on carbon doping (Figure 1.13). For this purpose, the calculated carrier concentrations at room

temperature and their known mobilities are used. A constant $As_{1<+ / 0>}$ (EL2)-concentration and an effective shallow donor concentration ($N_{\Sigma SD} - N_{\Sigma SA} \approx 10^{14} \text{ cm}^{-3}$) are assumed. The freezing temperature varies between 800 °C and 1010 °C. Experimental results are included into the graph for comparison.

The electrical resistivity increases linearly with the carbon concentration at $[C] > 2 \times 10^{14} \text{ cm}^{-3}$. In this region the above-given condition for semi-insulating behavior is met. The Fermi level is pinned at the deep $As_{1<+ / 0>}$ (EL2) donor. At about $C_{2<- / 0>} = [C] \approx 1 \times 10^{14} \text{ cm}^{-3}$ resistivity drops to a level of about $5 \times 10^3 \Omega \text{ cm}$. In this medium-resistivity region the carbon donor is compensated by the medium-deep oxygen donor, that is, the Fermi level is pinned at the effective level of oxygen. The EL2 concentration does not influence the electrical behavior.

As can be seen in Figure 1.13 resistivity is highly influenced by the freezing temperature. It decreases with decreasing freezing temperature. This is mainly caused by the decrease of the $As_{1<+ / 0>}$ (EL2) concentration due to a transition of arsenic into the interstitial sublattice As_3 . Furthermore, the calculations show an increase of the Ga vacancy concentration $Va_{1<0 / 3->}$ with increasing freezing temperature.

The Fermi-level effect on the thermodynamic data of defects in GaAs and its influence on the electrical behavior has been thoroughly studied in [28].

The Chemsage software package with the implementation of the SUBS model is a suitable tool for a chemical control of the GaAs crystal-growth process and for the understanding of the defect inventory of crystals and their physical properties.

1.5

Summary and Conclusions

Concept development and application of thermodynamic models comprise the following:

- definition of project and determination of the relevant components of the chemical system;
- selection of an appropriate thermodynamic software package;
- formulation of a thermodynamic-technological model, that is, description of phases and species to be included in the system and extraction of the required data from databases;
- test calculations with the option to modify the initial data and the boundary conditions of the model;
- calculation of the Gibbs free energies of separate phases, species and constituents;
- calculation of the Gibbs free energies for selected reactions;
- calculation of the multi-component system by minimization of the Gibbs free energy of the entire system;

- linking of the thermodynamic model with models describing reaction kinetics, mass and heat transport, etc.;
- verification and adjustment of the model;
- The modeling effort and the degree of approximation to reality will increase with the above steps;
- The applied *ChemSage* software package and the considered examples should demonstrate the possibilities and limitations of thermodynamic modeling of crystallization and crystal-growth processes.

In detail, there have been considered:

- the production of metallurgical silicon;
- reactions important for the silicon EFG process;
- carbon doping during GaAs single-crystal growth.

The results show that there are available thermodynamic software packages. However, comprehensive modeling of all aspects of crystal growth is still a vision.

Acknowledgments

The authors would like to thank P. Rudolph and U. Wunderwald for helpful discussions and critical reading of the manuscript. In addition, special thanks are expressed to A. Seidl, B. Weinert, and J. Friedrich. Eberhard Buhrig: I dedicate the part of the work formulated by me to my wife Renate†.

This work has been partly financed by BMBF 01-BM 631/2 and Freiburger Compound Materials GmbH.

References

- 1 Rosenberger, F. (1979) *Fundamentals of Crystal Growth I*, Springer, Berlin/Heidelberg/New York.
- 2 Wilke, K.-T. (1988) *Kristallzüchtung* (ed. J. Bohm), VEB Deutscher Verlag der Wissenschaft, Berlin.
- 3 Müller, G., and Friedrich, J. (2004) *J. Cryst. Growth*, **266**, 1–19.
- 4 Hurler, D.T.J. (1999) A comprehensive thermodynamic analysis of native point defect and dopant solubilities in Gallium Arsenide. *J. Appl. Phys.*, **85** (10), 6957–7023.
- 5 Jacobs, K. (2008) *Crystal Growth Technology* (eds H.J. Scheel and P. Capper), Wiley-VCH Verlag GmbH, Weinheim.
- 6 Bohm, J. (1995) *Realstruktur von Kristallen*, E. Schweitzerbart'sche Verlagsbuchhandlung, Stuttgart.
- 7 Hein, K., and Buhrig, E. (1983) *Kristallization aus Schmelzen*, VEB Deutscher Verlag für Grundstoffindustrie, Leipzig.
- 8 Roewer, G., and Buhrig, E. (2007) *50 Jahre Halbleitermaterialien in der Region Freiberg*, ZS für Freunde und Förderer der technischen Universität Freiberg.
- 9 Kuchar, L., and Drapala, J. (2008) *Metallurgy of Pure Metals*, Cambridge International Science Publishing.
- 10 Eriksson, G., and Hack, K. (1990) *ChemSage—a computer program for the*

- calculation of complex chemical equilibria. *Metall. Trans. B*, **21B**, 1013–1023.
- 11 Hack, K. (1996) The SGTE Casebook, Materials Modelling Series, The Institute of Materials, ISBN: 0 901716 74X.
 - 12 Thermo www.thermocalc.com (accessed 07-130N-2010).
 - 13 HSC www.hsc-chemistry.net (accessed 07-130N-2010).
 - 14 Redlich, O., and Kister, A.T. (1948) *Ind. Eng. Chem.*, **40**, 345. Muggianu, Y.M., Gambino, M., and Bros, J.P. (1975) *J. Chem. Phys.*, **72**, 83.
 - 15 Koukkari, P., Pajarre, R., and Hack, K. (2007) *Int. J. Mater. Res.*, **98**, 926–934.
 - 16 GTT <http://gttserver.lth.rwth-aachen.de/~cg/> (accessed 07-130N-2010).
 - 17 Petersen, S., and Hack, K. (2007) *Int. J. Mater. Res.*, **98**, 935–945.
 - 18 Rudolph, P. (1982) *Profilzüchtung von Einkristallen*, Akademie-Verlag, Berlin.
 - 19 Rudolph, P., and Jurisch, M. (1999) *J. Cryst. Growth*, **198/199**, 325–335.
 - 20 Wirbeleit, F. (1998) The atomic structure of point defects in semiconductors by improved EPR/ENDOR data analysis, PhD thesis, Technical University Mining Academy, Freiberg.
 - 21 Korb, J., Flade, T., Jurisch, M., Köhler, A., Reinhold, T., and Weinert, B. (1999) *J. Cryst. Growth*, **198/19**, 343–348.
 - 22 Oates, W.A., and Wenzl, H. (1998) *J. Cryst. Growth*, **191**, 303–312.
 - 23 Emori, H., Terashima, K., Orito, F., Kikuta, T., and Fukuda, T. (1984) *Semi-Insulating III–V Materials*, Kahnee-ta (eds D.C. Look and J.S. Blakemore), Shiva, Nantwich, p. 111.
 - 24 Eichler, S., Seidl, A., Börner, F., Kretzer, U., and Weinert, B. (2003) *J. Cryst. Growth*, **247**, 69–76.
 - 25 Oates, W.A., and Wenzl, H. (1992) *CALPHAD*, **16**, 73.
 - 26 Oates, W.A., and Wenzl, H. (1993) *CALPHAD*, **17**, 35.
 - 27 Oates, W.A., Eriksson, G., and Wenzl, H. (1995) Thermodynamic modelling of solid gallium arsenide. *J. Alloy. Compd.*, **220**, 48–52.
 - 28 Kretzer, U. (2007) *Punktdefekte und elektrische Kompensation in Galliumarsenid-Einkristallen*, PhD thesis, Technische Universität Chemnitz.